Genome-wide analyses of histone modifications and chromatin accessibility reveal the distinct genomic compartments in the Irish potato famine pathogen *Phytophthora infestans*

Han Chen[1#], Haidong Shu[1#], Yufeng Fang[2], Wenrui Song[1], Zhi Li[1], Yujie Fang[1], Yuanchao Wang[1] and Suomeng Dong[1]*

[1]Department of Plant Pathology and The Key Laboratory of Plant Immunity, Nanjing Agricultural University, Nanjing, China.

[2]GreenLight Biosciences Inc, Research Triangle Park, North Carolina, United States of America

#These authors contributed equally to this work

*Corresponding author, E-mail: smdong@njau.edu.cn

27

Abstract

Phytophthora infestans, the causal agent of potato late blight, is a devastating plant disease that leads to Irish potato famine and threatens world-wide food security. Despite the genome of *P. infestans* has provided fundamental resource for studying the aggressiveness of this pandemic pathogen, the epigenomes remain poorly understood. Here, utilizing liquid chromatography-tandem mass spectrometry (LC-MS/MS), we demonstrate post-translational modifications (PTM) at *P. infestans* core histone H3. The PTMs not only include these prevalent modifications in eukaryotes, and also some novel marks, such as H3K53me2 and H3K122me3. We focused on the trimethylations of H3K4, H3K9 and H3K27 and H3K36, and profiled *P. infestans* epigenomes employing Native Chromatin Immunoprecipitation followed by sequencing (N-ChIP-seq). In parallel, we mapped *P. infestans* chromomatin accessibility by Assay for Transposase-Accessible Chromatin with high-throughput sequencing (ATAC-seq). We found that adaptive genomic compartments display significantly higher levels of H3K9me3 and H3K27me3, and are generally in condense chromatin. Interestingly, we observed that genes encoding virulence factors, such as effectors, are enriched in open chromatin regions that barely have the four histone modifications. With a combination of genomic, epigenomic, transcriptomic strategies, our study illustrates the epigenetic states in *P. infestans*, which will help to study genomic functions and regulations in this pathogen.

48 Keywords: *Phytophthora infestans*, epigenetics, adaptive genome, histone modifications,

49 chromatin accessibility, gene expression

50

Author summary

Epigenetics play an important role in various biological processes of eukaryotes, including pathogenicity of plant pathogens. However, the epigenetic landscapes are marginally known in oomycetes that are fungal-like organisms and comprise lots of destructive plant pathogens. In this study, using the Irish potato famine pathogen *Phytophthora infestans* as a model, we conducted genome-wide studies of histone post modifications and chromatin accessibility, and demonstrate the relationship of gene expression and evolution with the epigenetic marks. We found that one of the most important classes of virulence proteins, effectors, are enriched in open chromatin regions that barely have eu- and hetero-chromatic marks. This study provides an overview of the oomycete epigenetic atlas, and advances our understanding of the regulation of virulence factors in plant pathogens.

Introduction

Late blight, a devastating disease is caused by *Phytophthora infestans* that strikes tomatoes and potatoes. The disease is notorious for trigging the 1840s Irish potato famine that resulted in the death of roughly one million people and the displacement of another million [1-3]. Today, *P. infestans* still remains a big threat to global plant health, causing ~US$6.5 billion losses annually [4-6]. Physiologically and morphologically *P. infestans* resembles filamentous fungi; however, it belongs to oomycete in the Stramenopila kingdom [7, 8]. A large number of oomycetes are destructive plant pathogens whose virulence extensively reply on virulence factors including extracellular toxins, hydrolytic enzymes and inhibitors, and effectors that can enter the cytoplasm of plant cells [9]. In particular, effectors are one of the most important factors that alter host physiology via initiating and allowing an infection to develop [10].

P. infestans has a large and complex genomes (~240 Mb), approximately 74% of the genome is composed of repeats, such as transposable elements [11]. Due to fast bursts of the transposable element activities, repeat-rich genomic regions are highly dynamic and prone to evolutionary changes at accelerated rates compared with the rest of the genome, which shapes the *P. infestans* genome “two-speed” [9, 12, 13]. Interestingly, these repeat-rich regions tend to harbor genes that contribute to virulence such as effector genes, which is critical for host adaptation [9, 12, 13]. To date, studies

have shown functions and evolutionary trajectory of the effector genes (reviewed in [9, 12, 14]), but how these genes are regulated is marginally known.

Epigenetic regulation is crucial for gene expression in the eukaryotes, which is generally influenced by chromatin states, non-coding RNA (ncRNA) and associated machinery, and modifications of DNA or histones, etc. [15, 16]. Importantly, pathogenicity traits, such as virulence [17], sexual reproduction [18], growth [19, 20], and drug resistance [21] have been shown to correlate with epigenetic regulation in eukaryotic pathogens. For instance, in the fungal kingdom, histone modifications, ncRNA mediated silencing and chromosome alterations have been shown to regulate the expression of virulence factors, antifungal drug resistance, and interaction with hosts during infections [21-26]. Similarly, in parasites, histone methylations were reported to control growth and virulence [17, 27]. In oomycetes, epigenetic studies are limited, but studies indicated that epigenetic profiles of oomycetes are distinctive comparing to other organisms, and that ncRNA, histone modifications and chromosome states contributed to virulence. Strikingly, the prevalent 5-cytosine methylation (5mC) is missing in *Phytophthora* species, instead 6-adenine methylation (6mA) is widely distributed across the genomes [28]. This unusual DNA methylation profile makes *Phytophthora* a great model to study the evolution of DNA methylation. Recently, ChIP-seq based on the H3 variant CenH3 (CENP-A) uncovered the centromeres in *P. sojae*, which lack H3K4me2 but embed within the heterochromatin marks H3K9me3 and H3K27me3 [29]. *In silico*, several histone

103 modification enzymes were identified in *Phytophthora*, including histone
104 acetyltransferases (HATs), deacetylases (HDACs) [30], some of which were involved in
105 metabolic and biosynthetic process, sexual reproduction and virulence [31, 32]. In
106 addition, gene silencing has been shown to be mediated by multiple different
107 mechanisms, and be an effective way for oomycete pathogens to modulate virulence
108 factors [33-35]. In *P. sojae,* transcription of the effector *Avr3a* was regulated by sRNA,
109 which led to transgenerational silencing [33], while silencing of another effector gene
110 *Avr1b* was correlated with H3K27me3 deposition [36]. In comparison, transgene-induced
111 silencing of the elicitor gene *INF1* involves chromatin alteration in *P. infestans*, *INF1*-
112 silenced strains harbor distinctive chromatin accessibility in the *INF1* loci [37, 38].

113 Despite evidence indicated that epigenetic processes affect growth, reproduction,
114 and virulence, we lack an overview of the epigenetic states especially the histone
115 modifications and chromosome states in oomycetes. In this study, we used *P. infestans*
116 as a model to systemically investigate the modifications of histone H3 by LC-MS/MS. We
117 focused on four important H3 modifications, H3K4me3, H3K9me3, H3K27me3 and
118 H3K36me3 that are hallmarks of eu-and hetero- chromatins, and profiled their
119 distributions across the genome. We also assessed the chromatin accessibility via
120 ATAC-seq. We demonstrate that the histone H3 methylations and chromatin accessibility
121 reflect *Phytophthora* genome structure, evolution and gene expression, and correlate
122 closely with virulence factors. These findings provide a new insight of oomycete

123 epigenome structures, and advance our understanding of oomycete genome
124 architectures, which sheds the light on future studies aimed at the epigenetic regulation
125 of plant pathogens.

126

127

Results

Detection of histone H3 post-translational modifications (PTMs) in *P. infestans*

We are interested in dissecting how *P. infestans* histone H3 are decorated. A previous study has cloned *P. sojae* H3 (PsH3), and demonstrated its predominant nuclear localization in the *P. sojae* transformants by fusing to GFP [39]. To identify histone H3 in *P. infestans*, we performed blast searches against *P. infestans* T30-4 genome employing the PsH3 ortholog. We found five H3 homologs (PITG_03551, PITG_05675, PITG_20725, PITG_06953 and PITG_13828) present in *P. infestans*. Closer examination of each H3 homologs revealed that PITG_13828 is CENP-A (CenH3), because of its sequence and structure similarity to the *P. sojae* CENP-A [29] (data not shown). Intriguingly, PITG_03551 and PITG_05675 (PiH3-1) have an identical amino acid sequence, but different nucleotide sequences, so did for PITG_20725 and PITG_06953 (PiH3-2) (S1 Fig., S2 Fig.).

To detect histone H3 post-translational modifications (PTMs) in *P. infestans*, we conducted high-performance liquid chromatography-mass spectrometry (HPLC-MS) employing trypsin digested histones. In total, we detected 23 PTM forms in *P. infestans* (Fig. 1A). Most reported H3 PTMs can be found over the *P. infestans* H3 tails, such as the conventional mono-, di-, and tri- methylation of lysine [K], acetylation of lysine, tyrosine and serine [K/T/S], and recently discovered butyrylation [K], 2-hydroxyisobutyrylation [K], crotonylation [K], hydroxylation [Y], and malonylation [K]. Of

148 note, we did not detect the acetylation of K27 that was a common acetylation form in
149 other organisms. On the other hand, we found some unique PMTs, such as di-
150 methylation at K53, tri-methylation at K122 (S3 Fig., S4 Fig.).

151 Further examination revealed distinct distributions of PTMs over the two H3
152 orthologues. Five PTM variations occurred across 10 amino acid substitutions between
153 two types of H3 (S3 Fig.). Acetylation and phosphorylation at T32 were detected in PiH3-
154 1. Besides, acetylation at T31, di-methylation at K53 and phosphorylation at Y78 were
155 detected in PiH3-2. It suggests different biological functions of H3 variants. Taken
156 together, these findings indicate that despite most of the histone PTMs are conserved in
157 *P. infestans* H3, several distinctive modification patterns are detected over several
158 residues.

159

160 **Profiling the genome-wide distribution of four histone H3 methylations and**
161 **chromatin accessibility**

162 To study the function of H3 PTMs, we focused on four histone methylations H3K4me3,
163 H3K36me3, H3K9me3 and H3K27me3, which are the hallmarks of transcriptionally
164 active euchromatin and transcriptionally silent heterochromatin. To validate the
165 expression of the four histone H3 methylations in *P. infestans*, we carried out western
166 blot using antibodies against these marks. As shown in S5 Fig., all the four histone
167 methylations were detected in *P. infestans*, but not in the *Escherichia coli* expressed H3

168 protein, as it lacks post histone modifications.

169 To study genome-wide distribution of H3K4me3, H3K36me3, H3K9me3, and
170 H3K27me3, we performed native chromatin immunoprecipitation (N-ChIP) employing the
171 four antibodies that were tested in western blot, followed by high-throughput Illumina
172 DNA sequencing. We generated high-quality map of each histone methylation with an
173 average of 30 million reads that were uniquely mapped to the *P. infestans* reference
174 genome (S6 Fig.). The four histone methylations displayed distinct distributions: For the
175 euchromatic marks, the majority of H3K4me3 peaks (62.6%) were distributed in gene
176 bodies, while 9.86% were in upstream of genes and 25.25% in intergenic regions (Fig.
177 2A). Moreover, we found thatH3K4me3 was highly enriched in transcription start sites
178 (TSS) (Fig. 2B). In comparison, H3K36me3 signals were scarce in upstream regions, but
179 were highly enriched in gene bodies (41.46%) and intergenic regions (54.02%) (Fig. 2A
180 and B). With respect to the heterochromatic marks H3K9me3 and H3K27me3, they
181 generally exhibited a similar distribution pattern: 95.44% H3K9me3 peaks and 96.01%
182 H3K27me3 peaks were localized in the intergenic regions (Fig. 2A, B and C).

183 One remarkable feature of heterochromatic marks is its association with repetitive
184 sequences [40]. In *P. sojae*, repetitive sequences, in particular, transposable elements
185 (TEs) were highly enriched with H3K27me3 and H3K9me3 [41]. Similarly, we found that
186 TEs in *P. infestans*, were highly enriched with H3K9me3 and H3K27me3, while lacked
187 H3K4me3 and H3K36me3 (Fig. 2C and S7A Fig.). Further investigation of different TE

188 families revealed that 55% H3K9me3 and 66% H3K27me3 signals were associated with
189 LTR retrotransposons that is the major TE family is the *P. infestans* genome (S7B Fig.).
190 Interestingly, the two heterochromatic marks exhibited quite different distribution over the
191 DNA transposons, with 16% H3K9me3 and 5% H3K27me3 (S7B, Fig).

192 To further investigate the chromatin state over the *P. infestans* genome, we profiled
193 the chromatin accessibility based on Assay for Transposase-Accessible Chromatin with
194 high-throughput sequencing (ATAC-seq). A high-quality chromatin accessibility map was
195 generated by aligning 100 million ATAC-seq reads uniquely to the reference genome (S6
196 Fig). We found that almost half of the ATAC-seq reads were mapped to the intergenic
197 regions, while 29.05% were in gene bodies and 12.59% were in upstream of genes (Fig.
198 2A). To examine the relationship between chromatin accessibility and the four histone
199 modifications, we implemented correlation analysis by PCA and heatmap. We found that
200 heterochromatin was anticorrelated with chromatin accessibility (Pearson co-efficiency
201 ranging from -0.15 to -0.23), while half euchromatin were somewhat correlated with
202 chromatin accessibility (Pearson co-efficiency ranging from 0.12 to 0.20) (S8 Fig, S9 Fig).
203 Comparing to H3K4me3, we found that the major ATAC-seq signals approximal gene
204 bodies were around 100 bp upstream of TSS, indicating that the open chromatin state of
205 promoter regions (Fig. 2B). It suggests the unique role of chromatin accessibility in
206 chromatin state defining compared with those four PTMs.

207

208 **Chromatin states strongly correlate with gene expression**

209 We next sought to examine the correlation of H3 modifications and chromatin
210 accessibility with gene expression. To determine expression levels of genes from the
211 same growth stage that was used for profiling chromatin states, we performed RNA-seq
212 from the *P. infestans* mycelial stage. We classified all *P. infestans* genes into six
213 categories from “Silent” to “Top” expression, based on their expression levels, (Fig. 2D).
214 We found that genes of higher expression were generally located in chromatin regions
215 that are more accessible, and that H3K4me3 and H3K36me3 were positively correlated
216 with gene expression (Fig. 2D) suggesting open chromatins and these euchromatic
217 histone marks are associated with active genes. In contrast, H3K9 and H3K27 tri-
218 methylations exhibited an anticorrelation with expression level, indicating these two
219 histone marks are associated with silencing (Fig. 2D). Genome browser views of
220 individual genomic locations also suggest a strong association of transcription activity
221 with chromatin accessibility and the four histone marks (Fig. 2C).

222 Collectively, these results illustrate that methylation of H3K4 and H3K36 is
223 associated with expressed genes, which are correlated with accessible chromatins;
224 while the methylation of H3K9 and H3K27 is enriched in areas of the genome that are
225 transcriptionally silent and are generally consisted of TEs, which tend to be closed
226 chromatin conformation.

227

Chromatin states reflect the bipartite genome structure

The genomes of *Phytophthora* species show a bipartite "two-speed" architecture that is consisted of gene-dense regions (GDRs), and gene-spare regions (GSRs) [11, 13, 42]. The GSR compartments are associated with accelerated gene evolution, serving as a cradle for adaptive evolution [11, 13, 42]. To investigate the relationship between chromatin state and the genome architecture, we measured the average level of each epigenetic state for genes located in GDRs and GSRs. We discovered that GSRs were enriched with the heterochromatic marks H3K9me3 and H3K27me3, and had condense chromatins, but lacked the euchromatic marks H3K4me3 and H3K36me3 (Fig. 3). In contrast, GDRs were enriched with the euchromatic marks H3K4me3 and H3K36me3, and were associated more accessible chromatin (Fig. 3). Thus, the epigenetic states display close correlation with the "two-speed" genome architecture.

Chromatin states are associated with the conservation of protein-coding genes

To address the connection between epigenetic state and protein evolution, we first sought to identify genes that were evolutionarily conserved in *P. infestans*. We selected 17 eukaryotic species including oomycetes, fungi, plants and animals, and measured the ratios of non-synonymous/synonymous codon substitution (dN/dS) for protein-coding genes. We found that the most conserved genes across eukaryotes had lowest dN/dS ratios, while the genes specific to *P. infestans* had highest dN/dS ratios, suggesting

248 species-specific genes are evolved later (S10A, B Fig.). In agreement with this
249 observation, high dN/dS density was also found in GSRs, further implying that the genes
250 in these regions were under higher evolutionary pressure (S10C Fig.).

251 Based on the gene evolution analysis, we examined the epigenetic states over each
252 protein-coding gene in *P*. *infestans*. We found that *P. infestans* specific genes had higher
253 level of H3K9me3 and H3K27me3, and were generally associated with condense
254 chromatin. In contrast, conserved genes had higher level of H3K4m3 and H3K36me3,
255 and were preferably associated with more open chromatin regions (Fig. 4A). We found
256 that genes that were under positive selection accumulated more H3K9me3 and
257 H3K27me3 signals, whereas the genes under purifying selection accumulated more
258 H3K4me3 and H3K36me3 (Fig. 4B). These findings are consistent with the chromatin
259 accessibility and methylation pattern of the “two speed” genome architecture that we
260 found above, namely the conserved genes are usually distributed in accessible GDR,
261 and thus are marked by H3K4me3 and H3K36me, whereas the rapidly evolved TEs are
262 enriched in the condensed GSR and thus associated with H3K9me3 and H3K27me3.

263

264 **Effector genes are enriched in highly accessible chromatin region with less**
265 **histone methylation level**

266 To characterize the functions of genes that were undergone histone methylation, we
267 performed gene ontology (GO) analysis. We found that histone methylations widely

contributed to biological processes (S11 Fig.). Interestingly, while the processes regulated by the euchromatic marks H3K4me3 and H3K36me3 were mostly different, these regulated by H3K9me3 and H3K27me3 were largely coincident (S11 Fig.), further indicating cross-talks may occur between the two heterochromatic marks for regulating gene expression. Notably, GO analysis indicated that histone modifications broadly contribute to pathogenesis related functions, such as pectate lyase activity and extracellular region, indicating the epigenetic regulation are critical for virulence. This prompted us to investigate the relationship between histone methylations and secreted proteins (secretome), in particular RxLR effectors [43, 44]. We found that comparing to other protein-coding genes, genes encoding secretome and RxLR effectors had overall higher H3K9me3 and H3K27me3and lower H3K4me3 and H3K36me3 densities (S12A, and S12B Fig.). It is possibly because the majority genes encoding RxLR effectors were repressed in mycelia stage.

To further investigate the role of chromatin state in regulating virulence, we generated a multivariate Hidden Markov Model based on the distribution of the four aforementioned histone marks and chromatin accessibility by chromHMM. *P. infestans* genome was divided into five distinct states including open chromatin (OC) that harbored ATAC-seq signals but lacked the four histone marks; strong transcription (ST) region that had abundant H3K4me3, H3K36me3, and ATAC-seq signals; H3K9me3 dominant repression region (H3K9DR); H3K27me3 dominant repression region (H3K27DR); and

288 quiescent (Quies) state that were absent of all the tested marks (Fig 5A). We found that
289 53.7% (868/1616) genes encoding secreted virulence factors, such as carbohydrate-
290 active enzymes (CAZyme) and various effector families such as Crinkler effectors (CRN),
291 necrosis- and ethylene-inducing-like proteins (NLP), small cysteine-rich effector proteins
292 (SCR) and RxLR, were associated with the OC and ST states (Fig. 5D, E). Interestingly,
293 despite OC state accounts for the smallest percentage (5.29% of the genome), 44%
294 RxLR effector-coding genes were associated with this state (Fig. 5E). A further analysis
295 showed CAZyme, NLP and RxLR gene families significantly enriched in OC state (Fig.
296 5F). GO analysis of genes from different chromatin state revealed, the GO items like
297 extracellular region, cell wall organization and pectin catabolic process were the most
298 enriched ones in OC state associated genes (S13 Fig.), suggesting the role of OC state
299 in *P. infestans* pathogenicity gene regulation.

300 To address how the expression profiles of the virulence genes correlated with the
301 OC state. We examined the transcriptomes of the *P. infestans* T30-4 strain at different
302 life/infection stages, such as mycelium (MY), 2 dpi (days post incubation) and 3 dpi. We
303 found that about half of the OC state-associated secreted virulence genes (CAZyme,
304 CRN, NLP, SCR and RxLR) displayed infection-induced pattern, for instance secreted
305 pectin monooxygenase encoding gene *PiAA17C* [45], and RxLR effector genes *Avrvnt1*,
306 *AvrSmira1 and Pi02860* [46-48] which are key virulence genes. In contrast, most ST
307 state-associated secreted virulence genes were relative highly expressed, although

some of them were infection-induced like *Avr3a* (Fig. 5G). To further explain the expression difference, we summarized the upregulation fold change of OC state and ST state-associated secreted virulence genes. Among 251 secreted virulence genes in OC state, 41.03% genes were 5-fold upregulated, and 35.45% genes were 10-fold unregulated at least in one infection stage. Otherwise, the ratio is lower in ST state (Fig. 5H). It suggests that OC state-associated virulence genes could be highly induced in infection stages. Altogether, our analyses implied the importance of OC state in virulence gene regulation.

Discussion

In this study, we identified the histone H3 PTMs in *P. infestans* by HPLC/MS, and generated an epigenetic atlas on basis of histone H3 methylations and chromatin accessibility. We found that most H3 PTMs were conserved in *P. infestans*. By examining the tri-methylation profiles of H3K4, H3K36, H3K9 and H3K27 and chromatin accessibility, we concluded that these chromatin states were closely associated with gene expression, genome structure, protein evolution, and virulence factors regulation. Our results provide evidence that epigenetic scenario is associated with pathogen genome in oomycete, and highlight chromatin state of virulence factors.

We found *Phytophthora* H3 proteins and H3 PTMs are slightly different from these reported in animal, plants and Protista, indicating dynamics of these highly conserved protein. With blast search, we found two H3 orthologues in *P. infestans*; however, with sequence composition and phylogenetic analyses, we cannot distinguish the canonical orthologue H3.1 and the variant H3.3 in *Phytophthora* (S2 Fig.). On the other hand, HPLC/MS revealed differences of PTM between the two *P. infestans* H3 orthologues (S3 Fig). This suggests that oomycete histone H3 may have a distinct evolutionary trajectory, additional experiment such as gene expression pattern examination in and outside of the S phase, and nucleosome assembly will help to clarify the two H3 variants in *Phytophthora*.

We found some unique modifications present in *P. infestans*, such as methylations at residues H3K53 and H3K122. H3K53me maybe species-specific, as in several organisms the residue 53 in H3 not lysine but arginine (S2B Fig.). In *Arabidopsis*, the H3K53 site was also reported to possess a modification; however, instead of methylation, it was 2-hydroxyisobutyrylation (Khib). Intriguingly, this unusual Khib modification contributed to the plant adaption to stress [49], suggesting H3K53me2 may also participate in some biological activities in *P. infestans*. Despite studies have shown that H3K122ac is a critical transcriptional regulator that defines genome-wide genetic elements and chromatin features associated with active transcription in mammalian cells [50], there is no report of H3K122 methylation, thus it will be of interest to examine its function in oomycetes. While most histone H3 PTMs reported to date can be found *in P. infestans*, we found acetylation of H3K27 and H3K36 are missing in the pathogen. Interestingly, histone acetyltransferase families that represent for H3K27ac and H3K36ac were identified [30], and a recent paper found both H3K27ac and H3K36ac in *P. infestans* [51]. It is possible that this modification level was too low to be detected in our mass spectrometry. Overall, we confirmed that large number of PTMs were presented in *P. infestans*, meanwhile, some unique PTMs were detected.

In *P. sojae*, it has been shown that H3K9me3 and H3K27me3 are generally coincident over the genome [29]. We generally observe a similar distribution pattern in *P. infestans*. Surprisingly, closer examination of TE demonstrated that the two

355 heterochromatic marks were separated over the DNA transposons (S7 Fig.), implying a
356 different mode may be used for silencing the types of TE. Another interesting features of
357 epigenetic marks we found in *P. infestans* is that H3K36me3 distributed over the gene
358 bodies of active genes (Fig. 2B), which is distinctive from strong methylation peak at the
359 3' end of the gene body in human and mouse, and strong peak at the 5' end of the gene
360 body *Arabidopsis* and rice, but is similar to the pattern in the brown alga *Ectocarpus*
361 *siliculosus*, yeast, and *C. elegans* [52, 53], suggesting divergent regulators and
362 mechanisms for establishing H3K36 methylation among species.

363 Genome-wide profiling of chromatin states provides insights into the unique genomic
364 compartments of plant pathogens. Principally, here we directly connected the chromatin
365 accessibility, histone methylation status and two-speed genome feature, and greatly
366 enriched the dimension of two-speed genome (Fig. 3). Similar to our results, high
367 enrichment of the heterochromatic marks H3K9me3 and H3K27me3, rather than the
368 euchromatic mark H3K4me2 was found in the rapidly evolved accessory chromosomes
369 in the wheat fungal pathogen *Zymoseptoria tritici* [54]. Recent research in the verticillium
370 wilt fungus *Verticillium dahliae* revealed adaptive lineage-specific genomic regions
371 contain many heterochromatin features, but more accessible than true heterochromatin
372 [55]. The heterochromatin features of adaptive genomic compartments in plant
373 pathogens remains a question that the formation and maintenance of these regions.
374 Mechanically, experimental evolution evidence proved that loss of H3K27me3 by

375 knockout methyltransferases Kmt6 drastically reduces the loss of accessory
376 chromosomes [56]. It explained why these regions are more susceptible to genetic
377 diversity. Further experimental research in *P. infestans* is needed to understand the
378 unique genomic compartments regulation. Besides, open chromatin sites reflect the
379 potential of recombination [57, 58], and *A. thaliana* showed that mutational rates are
380 significantly predicted by some epigenetic modifications [59]. It suggests that epigenetic
381 status is associated with evolutional hotspots. So, it' s reasonable to infer that chromatin
382 state details directly reflect sequence mutation and epimutation ratio in specific strains.
383 Higher resolution of two-speed genome and the molecular basis of genome architectural
384 reshaping are fascinating points to us.

385 Dissecting the chromatin state of genes encoding secreted virulence protein is one
386 of the key steps to illuminate *P. infestans* pathogenicity regulation. Interestingly, the GO
387 analysis indicated that gene related to extracellular region and pectin catabolic process
388 are enriched in the OC state (Fig. 5, S13 Fig.), meanwhile, those items was also
389 enriched in H3K9me3 and H3K27me3 methylated genes (S11 Fig.). We inferred that
390 those virulence genes involved in these GO items were not overlap and in different
391 regulation model. Firstly, most virulence genes in OC state had the potential to be
392 induced in infection stages, this kind of genes performed strong induction pattern due to
393 transcriptional releasing in infection stages (Fig. 5G, 5H). Secondly, the other virulence
394 genes were strongly repressed by methylation of histone lysine residues. Those kinds of

395 genes might be epigenetically regulated in *Phytophthora* [36], which was also observed
396 in other filamentous pathogens [60, 61]. Epigenetic silencing of TE by heterochromatin
397 marks to prevent TE proliferation in the TE-rich region is quiet common in filamentous
398 pathogen genomes [62], and we indeed found adjacent TEs around *RxLR* gene cluster
399 (S12 Fig.). Moreover, it has been accepted that epigenetic marks are tissue- and stage-
400 specific [63-65], revealing epigenomes of different stages and strains can dissect holistic
401 virulence gene regulation model. Here, we propose that functional regulatory elements
402 that contributed to establish and maintain normal chromatin state could be drug targets
403 to defect diseases. In conclusion, our findings reported herein provide clues for virulence
404 gene regulation mechanism investigation and pest management.
405

406 ## Materials and methods

407 Oomycete and fungal cultures

408 *P. infestans* strain T30-4, and *P. sojae* strain P6497 were used in the study. *P.*
409 *infestans* was routinely maintained on RSA/V8 medium at 18℃ in dark, and *P. sojae* on
410 10% V8 medium at 25℃ in dark [28].. *M. oryzae* strain Guy11 was regularly cultured in
411 CM medium at 28℃ [66].

412

413 LC-MS/MS analysis

414 Core histones were extracted from *P. infestans* mycelia employing EpiQuik Total
415 Histone Extraction Kit (EpiGentek, OP-0006-100), according to the manufacture
416 instruction. After being separated by 12% SDS-PAGE, proteins with ~ 17 kDa size were
417 extracted and analyzed by mass spectrum at Thermo Fisher. Given that H3 proteins
418 have multiple trypsin digestion site (lysine and arginine), a portion of sample was treated
419 with propionic anhydride (PA) to block trypsin digestion at the lysine sites to get maximal
420 sequencing read coverage. The trypsin digested peptides (derivatized and non-
421 derivatized) were injected to HLC/MS/MS (C18 HPLC column and Q Exactive HF-X
422 Mass Spectrometer), and the acquired MS/MS data was analyzed by the pFind3.0 [67]
423 with default parameters.

424

425 Protein extraction and western blot

426 To extract oomycete and fungal proteins, mycelia collected from liquid cultures of six
427 days old *P. infestans*, three days old *P. sojae*, and three days old *M. oryzae* were dried
428 by filter paper, and ground with mortars and pestles in liquid nitrogen. 800 µl lysis buffer
429 (1% SDS in TE buffer) was added into every 100 mg pulverized oomycete and fungal
430 tissue. Lysates were mixed by vortex for 30 min at 4℃. 200 µl supernatants were
431 collected after spun prepared for western blot. Protein samples were mixed with protein
432 loading buffer (Beyotime, P0015) and denatured at 95℃ for 10 min. To express PsH3 in
433 *E. coli*, the target gene (Ps_322070) was PCR amplified from *P. sojae*, and was cloned
434 into the plasmid pET32a using Vazyme ClonExpress II One Step Cloning Kit C112. The
435 resulting plasmid pET32a-PsH3 was introduced in *E. coli* BL21. The protein was
436 expressed at 30℃ for 8 hours in LB medium with 0.5 mM isopropyl β-D-Thiogalactoside
437 (IPTG) according to the manufacture instruction [68]. After sonication and centrifugation,
438 about 100 µl supernatant containing *E. coli* crude protein extract was used for western
439 blot. Antibodies H3K36me3 (abcam, ab9050), H3K27me3 (Millipore, 07-449), H3 (abcam,
440 ab1791), H3K4me3 (abcam, ab8580) and H3K9me3 (abcam, ab8898) were used as
441 primary antibodies against the relevant histone H3 modifications, and goat-anti-rabbit
442 IRDye 800CW antibody (Odyssey, no. 926-32211, Li-Cor) was as asecondary antibody.
443 The signals were exposure by laser imaging system (Odyssey, LI-COR company).

444

Phylogenetic analysis

H3 protein sequences from human (HsH3.1, accession number: NP_003520.1, HsH3.2, NP_066403.2, HsH3.3/NP_002098.1, HsCenP-A/NP_001035891.1), *Arabidopsis thaliana* (AtH3.1/NP_563838.1, AtH3.3/ NP_001329167.1, AtCenH3/NP_009564.1), *Neurospora crassa* (NcH3/CAA25761.1) and Saccharomyces cerevisiae (ScH3/NP_009564.1) were downloaded from NCBI. *Phytophthora* H2A sequence were from published paper [69]. Homologous gene blast was obtained by Seqhunter2 with an E value of 10^{-5}. Sequence alignment was performed by Bioedit software [70], and phylogenetic analysis was conducted by MEGA5 using neighbor-joining model and 10000 bootstrap replicates [71].

Native ChIP-seq, ATAC-seq and RNA-seq

Native ChIP experiments were performed as previously described [29, 36, 72]. Input and immunoprecipitated DNA samples were sequenced by BGI company as 50SE. To prepare ATAC-seq, *P. infestans* protoplasts were isolated according to refrenece [73]. Protoplast was stored at -80℃ using Nalgene 5100-0001C, and then sent to BGI for treatment [74]. In brief, lysing the cells and keep the cells on the ice all the time. Add Tn5 transposase to the cell suspension after cell lysis and then purify it. The DNA fragments were sequenced in BGI company as PE150. Infection samples (2 dpi and 3 dpi) were prepared as described [75]. RNA were extracted using Omega Total RNA Kit I according

465 to the manufacturer's manual, RNA-seq libraries were prepared by BGI company and
466 sequenced by BGISEQ-500.

467

468 High-throughput sequencing data analysis

469 Both ChIP-seq and ATAC-seq reads were polished by BGI prior to be released, and
470 thus were mapped to the *P. infestans* reference genome directly using Bowtie2 (v2.3.5.1)
471 [76] (see S6 Fig. for mappability). The aligned bam files were sorted and indexed by
472 samtools (version: 1.7) [77]. The ChIP-ed and input samples were analyzed with
473 DeepTools (v3.4.3) [78] ''bamCompare" to calculate normalized ChIP signals
474 (log2[$ChIP_{RPKM}$/$Input_{RPKM}$]),. ChIP-seq data was visualized using TBtools [79] and
475 Integrative Genome Viewer (IGV, v2.8.0) (https://software.broadinstitute.org/software/igv/)
476 [80]. ChIP-seq peaks were defined by MACS2 employing a default model for H3K4me3 ,
477 and a "--broad" model for H3K9me3, H3K27me3, and H3K36me3 [81, 82]. Peak
478 overlaps were conducted by "intersectBed" in bedtools [83]. To visualize the ATAC-seq
479 reads, BAM files were converted to bigwig format using "bamCompare" in DeepTools
480 with RPKM normalization. ATAC-seq data was visualized using TBtools [79] and IGV
481 v2.8.0 [80]. The ATAC-seq reads were shifted +4 on the positive strands and -5 on the
482 negative strands using deepTools software, and then ATAC-seq peaks were defined by
483 MACS2 in default model. Peak overlap was conducted by "intersectBed" in bedtools.
484 RNA-seq reads were polished by BGI prior to be released. To generate mRNA profiles,

485 the RNA-seq reads were aligned to the genomes using HISAT2 (version 2.1.0) [84] , and
486 the resulting files (.bam) were sorted and indexed by samtools (version 1.9) [77]. The
487 bam file was converted to .tdf for visualization using IGV. Gene expression data were
488 calculated by StringTie v2.1.2 [85] and was presented as FPKM values.

489

490 Other analysis

491 PCA plot and heatmap clustering of ChIP-seq and ATAC-seq was using “plotPCA”
492 and “plotCorrelation” in deepTools. Overlap of ATAC peak and ChIP-seq were conducted
493 by “intersectBed” in bedtools. The Pearson correlation computation was used in
494 heatmap clustering. The chromatin state was defined by chromHMM [86] in “BinarizeBed”
495 model using MACS2 peak files. GO enrichment was analyzed by R package
496 clusterprofile v3.14.3 by universal enrichment analyzer “enricher” and “compareCluster”
497 [87]. Gene conservation analysis among species was performed by OrthoMCL v2.0.9 by
498 default parameters [88]. Protein conservation was based on 17 eukaryotic species
499 including oomycetes, fungi, plants and animals, and divided the *P. infestans* coding-
500 genes into four groups (Eukaryote, Oomycete, *Phytophthora* and *P. infestans*), each of
501 which has 1157, 3064, 5680 and 2483 genes. Eukaryote group contains protein-coding
502 genes that conserved among all 17 species. Oomycete group contains protein-coding
503 genes that conserved among 10 oomycetes besides genes in eukaryote group.

Phytophthora group and *P. infestans* specific groups can be inferred like this. The Sankey plot was performed by R package networkD3 [89].

Funding

This work was supported by the National Natural Science Foundation of China (NSFC) 31721004 and 32100158, China Postdoctoral Science Foundation 2019TQ0156 and Natural Science Foundation of Jiangsu Province BK20200538.

Competing interests

The authors have declared that no competing interests exist.

Acknowledgments

We are grateful to the Bioinformatics Center at Nanjing Agricultural University for support of the bioinformatics analysis. We thank the NJAU oomycete research group for valuable discussion.

References

1. Kinealy C. This great calamity : the Irish famine 1845-52. 2006.

2. Turner RS. After the famine: Plant pathology, Phytophthora infestans, and the late blight of potatoes, 1845–-1960. Historical Studies in the Physical and Biological Sciences. 2005;35(2):341-70. doi: 10.1525/hsps.2005.35.2.341.

3. McDonough T. Mapping the Great Irish Famine. JSTOR; 2001.

4. Fones HN, Bebber DP, Chaloner TM, Kay WT, Steinberg G, Gurr SJ. Threats to global food security from emerging fungal and oomycete crop pathogens. Nature Food. 2020;1(6):332-42. doi: 10.1038/s43016-020-0075-0.

5. Savary S, Willocquet L, Pethybridge SJ, Esker P, McRoberts N, Nelson A. The global burden of pathogens and pests on major food crops. Nat Ecol Evol. 2019;3(3):430-9. Epub 2019/02/06. doi: 10.1038/s41559-018-0793-y. PubMed PMID: 30718852.

6. Campos H, Ortiz O. The potato crop: its agricultural, nutritional and social contribution to humankind: Springer Nature; 2020.

7. Burki F, Roger AJ, Brown MW, Simpson AGB. The New Tree of Eukaryotes. Trends in Ecology & Evolution. 2020;35(1):43-55. doi: 10.1016/j.tree.2019.08.008.

8. Thines M, Kamoun S. Oomycete-plant coevolution: recent advances and future prospects. Current opinion in plant biology. 2010;13(4):427-33. doi: 10.1016/j.pbi.2010.04.001. PubMed PMID: 20447858.

9. Jiang RH, Tyler BM. Mechanisms and evolution of virulence in oomycetes. Annual review of

phytopathology. 2012;50:295-318. doi: 10.1146/annurev-phyto-081211-172912. PubMed PMID: 22920560.

10. Wawra S, Belmonte R, Lobach L, Saraiva M, Willems A, van West P. Secretion, delivery and function of oomycete effector proteins. Current opinion in microbiology. 2012;15(6):685-91. Epub 2012/11/28. doi: 10.1016/j.mib.2012.10.008. PubMed PMID: 23177095.

11. Haas BJ, Kamoun S, Zody MC, Jiang RH, Handsaker RE, Cano LM, et al. Genome sequence and analysis of the Irish potato famine pathogen Phytophthora infestans. Nature. 2009;461(7262):393-8. Epub 2009/09/11. doi: 10.1038/nature08358. PubMed PMID: 19741609.

12. Raffaele S, Kamoun S. Genome evolution in filamentous plant pathogens: why bigger can be better. Nature reviews Microbiology. 2012;10(6):417-30. doi: 10.1038/nrmicro2790. PubMed PMID: 22565130.

13. Dong S, Raffaele S, Kamoun S. The two-speed genomes of filamentous pathogens: waltz with plants. Current opinion in genetics & development. 2015;35:57-65. doi: 10.1016/j.gde.2015.09.001. PubMed PMID: 26451981.

14. Birch PR, Boevink PC, Gilroy EM, Hein I, Pritchard L, Whisson SC. Oomycete RXLR effectors: delivery, functional redundancy and durable disease resistance. Current opinion in plant biology. 2008;11(4):373-9.

15. Goldberg AD, Allis CD, Bernstein E. Epigenetics: a landscape takes shape. Cell. 2007;128(4):635-8. Epub 2007/02/27. doi: 10.1016/j.cell.2007.02.006. PubMed PMID: 17320500.

16. Allis CD, Jenuwein T. The molecular hallmarks of epigenetic control. Nature reviews

561 Genetics. 2016;17(8):487-500. Epub 2016/06/28. doi: 10.1038/nrg.2016.59. PubMed PMID:
562 27346641.
563 17. Jiang L, Mu J, Zhang Q, Ni T, Srinivasan P, Rayavara K, et al. PfSETvs methylation of
564 histone H3K36 represses virulence genes in Plasmodium falciparum. Nature.
565 2013;499(7457):223-7. Epub 2013/07/05. doi: 10.1038/nature12361. PubMed PMID: 23823717;
566 PubMed Central PMCID: PMC3770130.
567 18. Scaduto CM, Kabrawala S, Thomson GJ, Scheving W, Ly A, Anderson MZ, et al. Epigenetic
568 control of pheromone MAPK signaling determines sexual fecundity in Candida albicans.
569 Proceedings of the National Academy of Sciences of the United States of America.
570 2017;114(52):13780-5. doi: 10.1073/PNAS.1711141115.
571 19. Mittelsten Scheid O, Zhang W, Huang J, Cook DE. Histone modification dynamics at H3K27
572 are associated with altered transcription of in planta induced genes in Magnaporthe oryzae. PLoS
573 genetics. 2021;17(2):e1009376. doi: 10.1371/journal.pgen.1009376.
574 20. Rai LS, Singha R, Brahma P, Sanyal K. Epigenetic determinants of phenotypic plasticity in
575 Candida albicans. Fungal Biology Reviews. 2018;32(1):10-9. doi: 10.1016/j.fbr.2017.07.002.
576 21. Calo S, Shertz-Wall C, Lee SC, Bastidas RJ, Nicolas FE, Granek JA, et al. Antifungal drug
577 resistance evoked via RNAi-dependent epimutations. Nature. 2014;513(7519):555-8. doi:
578 10.1038/nature13575. PubMed PMID: 25079329; PubMed Central PMCID: PMC4177005.
579 22. Connolly LR, Smith KM, Freitag M. The Fusarium graminearum histone H3 K27
580 methyltransferase KMT6 regulates development and expression of secondary metabolite gene

581 clusters. PLoS genetics. 2013;9(10):e1003916. Epub 2013/11/10. doi:
582 10.1371/journal.pgen.1003916. PubMed PMID: 24204317; PubMed Central PMCID:
583 PMC3814326.

584 23. Galazka JM, Freitag M. Variability of chromosome structure in pathogenic fungi--of 'ends and
585 odds'. Current opinion in microbiology. 2014;20:19-26. doi: 10.1016/j.mib.2014.04.002. PubMed
586 PMID: 24835423; PubMed Central PMCID: PMC4133287.

587 24. Liu Y, Liu N, Yin Y, Chen Y, Jiang J, Ma Z. Histone H3K4 methylation regulates hyphal
588 growth, secondary metabolism and multiple stress responses in Fusarium graminearum.
589 Environmental microbiology. 2015;17(11):4615-30. doi: 10.1111/1462-2920.12993. PubMed
590 PMID: 26234386.

591 25. Collemare J, Seidl MF. Chromatin-dependent regulation of secondary metabolite
592 biosynthesis in fungi : is the picture complete? fems microbiology reviews. 2019;43(6):591-607.
593 doi: 10.1093/FEMSRE/FUZ018.

594 26. Torres-Garcia S, Yaseen I, Shukla M, Audergon PNCB, White SA, Pidoux AL, et al.
595 Epigenetic gene silencing by heterochromatin primes fungal resistance. Nature. 2020. doi:
596 10.1038/s41586-020-2706-x.

597 27. Scherf A, Lopez-Rubio JJ, Riviere L. Antigenic Variation in Plasmodium falciparum. Annual
598 review of microbiology. 2008;62(1):445-70. doi: 10.1146/annurev.micro.61.080706.093134.
599 PubMed PMID: WOS:000259968000024.

600 28. Chen H, Shu H, Wang L, Zhang F, Li X, Ochola SO, et al. Phytophthora methylomes are

601 modulated by 6mA methyltransferases and associated with adaptive genome regions. Genome
602 Biol. 2018;19(1):181. doi: 10.1186/s13059-018-1564-4. PubMed PMID: 30382931; PubMed
603 Central PMCID: PMC6211444.
604 29. Fang Y, Coelho MA, Shu H, Schotanus K, Thimmappa BC, Yadav V, et al. Long transposon-
605 rich centromeres in an oomycete reveal divergence of centromere features in Stramenopila-
606 Alveolata-Rhizaria lineages. PLoS genetics. 2020;16(3):e1008646. doi:
607 10.1371/journal.pgen.1008646. PubMed PMID: 32150559.
608 30. Wang X, Guo L, Han M, Shan K. Diversity, evolution and expression profiles of histone
609 acetyltransferases and deacetylases in oomycetes. BMC genomics. 2016;17(1):927.
610 31. Wang X-W, Lv J-L, Shi Y-R, Guo L-Y. Comparative Transcriptome Analysis Revealed Genes
611 Regulated by Histone Acetylation and Genes Related to Sex Hormone Biosynthesis in
612 Phytophthora infestans. Frontiers in genetics. 2020;11. doi: 10.3389/fgene.2020.00508.
613 32. Tzelepis G, Hoden KP, Fogelqvist J, Asman AKM, Vetukuri RR, Dixelius C. Dominance of
614 Mating Type A1 and Indication of Epigenetic Effects During Early Stages of Mating in
615 Phytophthora infestans. Front Microbiol. 2020;11:252. Epub 2020/03/11. doi:
616 10.3389/fmicb.2020.00252. PubMed PMID: 32153537; PubMed Central PMCID:
617 PMCPMC7046690.
618 33. Qutob D, Chapman BP, Gijzen M. Transgenerational gene silencing causes gain of virulence
619 in a plant pathogen. Nature communications. 2013;4:1349. Epub 2013/01/17. doi:
620 10.1038/ncomms2354. PubMed PMID: 23322037; PubMed Central PMCID: PMC3562452.

621 34. Kasuga T, Gijzen M. Epigenetics and the evolution of virulence. Trends in microbiology.
622 2013;21(11):575-82. Epub 2013/10/08. doi: 10.1016/j.tim.2013.09.003. PubMed PMID: 24095304.
623 35. Shrestha SD, Chapman P, Zhang Y, Gijzen M. Strain Specific Factors Control Effector Gene
624 Silencing in Phytophthora sojae. PloS one. 2016;11(3):e0150530. doi:
625 10.1371/journal.pone.0150530. PubMed PMID: 26930612; PubMed Central PMCID:
626 PMC4773254.
627 36. Wang L, Chen H, Li J, Shu H, Zhang X, Wang Y, et al. Effector gene silencing mediated by
628 histone methylation underpins host adaptation in an oomycete plant pathogen. Nucleic Acids Res.
629 2020;48(4):1790-9. doi: 10.1093/nar/gkz1160. PubMed PMID: 31819959; PubMed Central
630 PMCID: PMC7039004.
631 37. van West P, Kamoun S, van 't Klooster JW, Govers F. Internuclear gene silencing in
632 Phytophthora infestans. Molecular cell. 1999;3(3):339-48. Epub 1999/04/13. doi: 10.1016/s1097-
633 2765(00)80461-x. PubMed PMID: 10198636.
634 38. van West P, Shepherd SJ, Walker CA, Li S, Appiah AA, Grenville-Briggs LJ, et al.
635 Internuclear gene silencing in Phytophthora infestans is established through chromatin
636 remodelling. Microbiology. 2008;154(Pt 5):1482-90. doi: 10.1099/mic.0.2007/015545-0. PubMed
637 PMID: 18451057.
638 39. Fang Y, Jang HS, Watson GW, Wellappili DP, Tyler BM. Distinctive nuclear localization
639 signals in the oomycete *Phytophthora sojae*. Front Microbiol. 2017;8:10. Epub 2017/02/18. doi:
640 10.3389/fmicb.2017.00010. PubMed PMID: 28210240; PubMed Central PMCID:

641 PMCPMC5288373.

642 40. Clark DP, Pazdernik NJ. Chapter 8 - Genomics and Gene Expression. In: Clark DP,

643 Pazdernik NJ, editors. Biotechnology (Second Edition). Boston: Academic Cell; 2016. p. 249-94.

644 41. Fang YF, Coelho MA, Shu H, Schotanus K, Thimmappa BC, Yadav V, et al. Long

645 transposon-rich centromeres in an oomycete reveal divergence of centromere features in

646 Stramenopila-Alveolata-Rhizaria lineages. bioRxiv. 2019:765032. doi: 10.1101/765032.

647 42. Raffaele S, Farrer RA, Cano LM, Studholme DJ, MacLean D, Thines M, et al. Genome

648 evolution following host jumps in the Irish potato famine pathogen lineage. Science.

649 2010;330(6010):1540-3. Epub 2010/12/15. doi: 10.1126/science.1193070. PubMed PMID:

650 21148391.

651 43. Wang Y, Tyler BM, Wang Y. Defense and Counterdefense During Plant-Pathogenic

652 Oomycete Infection. Annual review of microbiology. 2019;73:667-96. Epub 2019/06/22. doi:

653 10.1146/annurev-micro-020518-120022. PubMed PMID: 31226025.

654 44. Vleeshouwers VG, Raffaele S, Vossen JH, Champouret N, Oliva R, Segretin ME, et al.

655 Understanding and exploiting late blight resistance in the age of effectors. Annual review of

656 phytopathology. 2011;49:507-31. Epub 2011/06/15. doi: 10.1146/annurev-phyto-072910-095326.

657 PubMed PMID: 21663437.

658 45. Sabbadin F, Urresti S, Henrissat B, Avrova AO, Welsh LRJ, Lindley PJ, et al. Secreted

659 pectin monooxygenases drive plant infection by pathogenic oomycetes. science.

660 2021;373(6556):774-9. doi: 10.1126/SCIENCE.ABJ1342.

661 46. Gao C, Xu H, Huang J, Sun B, Zhang F, Savage Z, et al. Pathogen manipulation of
662 chloroplast function triggers a light-dependent immune recognition. Proceedings of the National
663 Academy of Sciences of the United States of America. 2020;117(17):9613-20. doi:
664 10.1073/PNAS.2002759117.
665 47. Yang L, McLellan H, Naqvi S, He Q, Boevink PC, Armstrong M, et al. Potato NPH3/RPT2-
666 like protein StNRL1, targeted by a Phytophthora infestans RXLR effector, is a susceptibility factor.
667 Plant physiology. 2016;171(1):645-57. doi: 10.1104/PP.16.00178.
668 48. Stefańczyk E, Sobkowiak S, Brylińska M, Śliwka J. Expression of the Potato Late Blight
669 Resistance Gene Rpi-phu1 and Phytophthora infestans Effectors in the Compatible and
670 Incompatible Interactions in Potato. phytopathology. 2017;107(6):740-8. doi: 10.1094/PHYTO-09-
671 16-0328-R.
672 49. Zheng L, Li C, Ma X, Zhou H, Liu Y, Wang P, et al. Functional interplay of histone lysine 2-
673 hydroxyisobutyrylation and acetylation in Arabidopsis under dark-induced starvation. Nucleic
674 Acids Research. 2021;49(13):7347-60. doi: 10.1093/nar/gkab536.
675 50. Tropberger P, Pott S, Keller C, Kamieniarz-Gdula K, Caron M, Richter F, et al. Regulation of
676 transcription through acetylation of H3K122 on the lateral surface of the histone octamer. Cell.
677 2013;152(4):859-72.
678 51. Grau-Bové X, Navarrete C, Chiva C, Pribasnig T, Antó M, Torruella G, et al. Comparative
679 proteogenomics deciphers the origin and evolution of eukaryotic chromatin. 2021.
680 52. Bourdareau S, Tirichine L, Lombard B, Loew D, Scornet D, Wu Y, et al. Histone

681 modifications during the life cycle of the brown alga Ectocarpus. Genome Biology. 2021;22(1). doi:
682 10.1186/s13059-020-02216-8.
683 53. Liu B, Liu Y, Wang B, Luo Q, Shi J, Gan J, et al. The transcription factor OsSUF4 interacts
684 with SDG725 in promoting H3K36me3 establishment. Nature communications. 2019;10(1). doi:
685 10.1038/s41467-019-10850-5.
686 54. Schotanus K, Soyer JL, Connolly LR, Grandaubert J, Happel P, Smith KM, et al. Histone
687 modifications rather than the novel regional centromeres of Zymoseptoria tritici distinguish core
688 and accessory chromosomes. Epigenetics & Chromatin. 2015;8(1). doi: 10.1186/s13072-015-
689 0033-5.
690 55. Cook DE, Kramer HM, Torres DE, Seidl MF, Thomma BP. A unique chromatin profile defines
691 adaptive genomic regions in a fungal plant pathogen. Elife. 2020;9. doi: 10.7554/eLife.62208.
692 PubMed PMID: 33337321.
693 56. Möller M, Schotanus K, Soyer JL, Haueisen J, Happ K, Stralucke M, et al. Destabilization of
694 chromosome structure by histone H3 lysine 27 methylation. PLoS genetics. 2019;15(4). doi:
695 10.1371/JOURNAL.PGEN.1008093.
696 57. Rodgers-Melnick E, Vera DL, Bass HW, Buckler ES. Open chromatin reveals the functional
697 maize genome. Proceedings of the National Academy of Sciences. 2016;113(22):E3177-E84. doi:
698 10.1073/pnas.1525244113.
699 58. Spruce C, Dlamini S, Ananda G, Bronkema N, Tian H, Paigen K, et al. HELLS and PRDM9
700 form a pioneer complex to open chromatin at meiotic recombination hot spots. Genes &

Development. 2020;34(5-6):398-412. doi: 10.1101/gad.333542.119.

59. Monroe JG, Srikant T, Carbonell-Bejerano P, Exposito-Alonso M, Weng M-L, Rutter MT, et al. Mutation bias shapes gene evolution in Arabidopsis thaliana. BioRxiv. 2020. doi: 10.1101/2020.06.17.156752.

60. Chen H, Raffaele S, Dong S. Silent control: microbial plant pathogens evade host immunity without coding sequence changes. FEMS Microbiol Rev. 2021. Epub 2021/01/14. doi: 10.1093/femsre/fuab002. PubMed PMID: 33440001.

61. Soyer JL, El Ghalid M, Glaser N, Ollivier B, Linglin J, Grandaubert J, et al. Epigenetic control of effector gene expression in the plant pathogenic fungus Leptosphaeria maculans. PLoS genetics. 2014;10(3):e1004227. Epub 2014/03/08. doi: 10.1371/journal.pgen.1004227. PubMed PMID: 24603691; PubMed Central PMCID: PMC3945186.

62. Fouche S, Plissonneau C, Croll D. The birth and death of effectors in rapidly evolving filamentous pathogen genomes. Current opinion in microbiology. 2018;46:34-42. doi: 10.1016/j.mib.2018.01.020. PubMed PMID: 29455143.

63. Roy S, Ernst J, Kharchenko PV, Kheradpour P, Negre N, Eaton ML, et al. Identification of Functional Elements and Regulatory Circuits by Drosophila modENCODE. Science. 2010;330(6012):1787-97. doi: 10.1126/science.1198374.

64. Gerstein MB, Lu ZJ, Van Nostrand EL, Cheng C, Arshinoff BI, Liu T, et al. Integrative Analysis of the Caenorhabditis elegans Genome by the modENCODE Project. Science. 2010;330(6012):1775-87. doi: 10.1126/science.1196914.

721 65. Shen Y, Yue F, McCleary DF, Ye Z, Edsall L, Kuan S, et al. A map of the cis-regulatory
722 sequences in the mouse genome. Nature. 2012;488(7409):116-20. doi: 10.1038/nature11243.
723 66. Qian B, Su X, Ye Z, Liu X, Liu M, Shen D, et al. MoErv29 promotes apoplastic effector
724 secretion contributing to virulence of the rice blast fungus Magnaporthe oryzae. new phytologist.
725 2021. doi: 10.1111/NPH.17851.
726 67. Chi H, Liu C, Yang H, Zeng W-F, Wu L, Zhou W-J, et al. Comprehensive identification of
727 peptides in tandem mass spectra using an efficient open search engine. Nature biotechnology.
728 2018;36(11):1059-61. doi: 10.1038/NBT.4236.
729 68. Sambrook J, Fritsch EF, Maniatis T. Molecular Cloning: A Laboratory Manual2001 1/15/2001.
730 69. Wang X, Guo L. Sequence analysis and expression patterns of histone H2A variants in
731 Phytophthora infestans. chinese journal of biotechnology. 2016;32(11):1564-75. doi:
732 10.13345/J.CJB.160109.
733 70. Alzohairy AM. BioEdit: An important software for molecular biology. 2011.
734 71. Tamura K, Peterson DS, Peterson N, Stecher G, Nei M, Kumar S. MEGA5: Molecular
735 Evolutionary Genetics Analysis Using Maximum Likelihood, Evolutionary Distance, and Maximum
736 Parsimony Methods. Molecular biology and evolution. 2011;28(10):2731-9.
737 72. Li HY, Wang HN, Jing MF, Zhu JY, Guo BD, Wang Y, et al. A Phytophthora effector recruits
738 a host cytoplasmic transacetylase into nuclear speckles to enhance plant susceptibility. Elife.
739 2018;7. doi: ARTN e40039
740 10.7554/eLife.40039. PubMed PMID: WOS:000450804600001.

741 73. Zhao Y, Li Y, Qiu M, Ma W, Wang Y. Generating Gene Silenced Mutants in Phytophthora
742 sojae. In: Ma W, Wolpert T, editors. Plant Pathogenic Fungi and Oomycetes: Methods and
743 Protocols. New York, NY: Springer New York; 2018. p. 275-86.
744 74. Huang L, Li X, Dong L, Wang B, Pan L. Profiling of chromatin accessibility identifies
745 transcription factor binding sites across the genome of Aspergillus species. bmc biology.
746 2021;19(1). doi: 10.1186/S12915-021-01114-0.
747 75. Zhang F, Chen H, Zhang XJ, Gao CY, Huang J, Lu L, et al. Genome Analysis of Two Newly
748 Emerged Potato Late Blight Isolates Sheds Light on Pathogen Adaptation and Provides Tools for
749 Disease Management. Phytopathology. 2021;111(1):96-107. Epub 2020/10/08. doi:
750 10.1094/Phyto-05-20-0208-Fi. PubMed PMID: WOS:000614285700009.
751 76. Langmead B, Salzberg SL. Fast gapped-read alignment with Bowtie 2. Nature methods.
752 2012;9(4):357-9. doi: 10.1038/NMETH.1923.
753 77. Li H, Handsaker B, Wysoker A, Fennell T, Ruan J, Homer N, et al. The Sequence
754 Alignment/Map format and SAMtools. bioinformatics. 2009;25(16):2078-9. doi:
755 10.1093/BIOINFORMATICS/BTP352.
756 78. Ramírez F, Dündar F, Diehl S, Grüning BA, Manke T. deepTools: a flexible platform for
757 exploring deep-sequencing data. Nucleic acids research. 2014;42:187-91. doi:
758 10.1093/NAR/GKU365.
759 79. Chen C, Chen H, Zhang Y, Thomas HR, Frank MH, He Y, et al. TBtools: An Integrative
760 Toolkit Developed for Interactive Analyses of Big Biological Data. Molecular plant.

761 2020;13(8):1194-202. doi: 10.1016/J.MOLP.2020.06.009.

762 80. Robinson JT, Thorvaldsdóttir H, Winckler W, Guttman M, Lander ES, Getz G, et al.

763 Integrative genomics viewer. Nature biotechnology. 2011;29(1):24-6. doi: 10.1038/NBT.1754.

764 81. Gaspar JM. Improved peak-calling with MACS2. 2018.

765 82. Zhang Y, Liu T, Meyer CA, Eeckhoute J, Johnson DS, Bernstein BE, et al. Model-based

766 Analysis of ChIP-Seq (MACS). genome biology. 2008;9(9):1-9. doi: 10.1186/GB-2008-9-9-R137.

767 83. Quinlan AR, Hall IMJB. BEDTools: a flexible suite of utilities for comparing genomic features.

768 2010;26(6):841-2.

769 84. Kim D, Langmead B, Salzberg SL. HISAT: a fast spliced aligner with low memory

770 requirements. Nature methods. 2015;12(4):357-60. doi: 10.1038/NMETH.3317.

771 85. Pertea M, Pertea GM, Antonescu CM, Chang TC, Mendell JT, Salzberg SL. StringTie

772 enables improved reconstruction of a transcriptome from RNA-seq reads. Nature biotechnology.

773 2015;33(3):290-5. doi: 10.1038/NBT.3122.

774 86. Ernst J, Kellis M. ChromHMM: automating chromatin-state discovery and characterization.

775 Nature methods. 2012;9(3):215-6. doi: 10.1038/nmeth.1906.

776 87. Yu G, Wang LG, Han Y, He QY. clusterProfiler: an R Package for Comparing Biological

777 Themes Among Gene Clusters. omics a journal of integrative biology. 2012;16(5):284-7. doi:

778 10.1089/OMI.2011.0118.

779 88. Li L, Stoeckert CJ, Roos DS. OrthoMCL: identification of ortholog groups for eukaryotic

780 genomes. genome research. 2003;13(9):2178-89. doi: 10.1101/GR.1224503.

781 89. Allaire JJ, Gandrud C, Russell K, Yetman CJ. D3 JavaScript Network Graphs from R [R

782 package networkD3 version 0.4]. 2017.

783

Figure legends

Fig. 1 Histone H3 modifications identified in *P. infestans*. Schematic showing various *P. infestans* H3 (PiH3) PTMs that was detected by HPLC-MS/MS. Numbers at top of the PiH3 amino acid sequence indicate the positions of residues. Dots with different colors denote different types of PTMs, and the red ones at the top of K represent lysine tri-methylation.

Fig. 2 Distribution of four histone H3 methylations and chromatin accessibility.

(A). Heatmap showed the distribution of ChIP-seq and ATAC-seq peak. upstream was defined as -800 bp before start code, downstream was defined as +400 bp after stop code. Submits of peaks in S6C Fig. were used. (B). line plot showed the distribution of four histone H3 methylations and chromatin accessibility across gene, -1 kb to +1 kb region were included. (C). Representative snapshot of H3 methylations and ATAC-seq statue. The snapshot was collected from IGV software. (D), Accessible chromatin, H3K4me3 and H3K36me3 are associated with highly expressed genes, meanwhile, H3K9me3 and H3K27me3 are associated silenced genes.

Fig. 3 Distribution of H3 methylations and chromatin accessibility reflects the bipartite genome structure.

803 Heatmap analyses showed higher H3K9me3 and H3K27me3 in GSR, meanwhile, higher
804 ATAC-seq, H3K4me3 and H3K36me3 density in GDR. The dotted line highlights GSR.
805 Gradient color represents gene number is gene density plot, and gradient color in other
806 plot represent the average normalized ATAC-seq or H3 methylation signal.

807

808 **Fig. 4 Histone H3 methylations and chromatin accessibility are associated with**
809 **evolution of the protein-coding genes.**

810 H3K9me3 and H3K27me3 were abundant in *P. infestans* specific genes (A) and fast
811 evolved genes (B) with generally condense chromatin, whereas higher H3K4m3 and
812 H3K36me3 preferably associated with conserved genes which were located in more
813 accessible chromatin regions. In (A), Pink, purple, blue and green represent eukaryote,
814 oomycete, Phytophthora, and P. infestans specific gene groups, respectively. In (B), all
815 protein-coding genes were divided into two categories based on their dN/dS ratios, their
816 methylation and ATAC-seq density were compared. The number of genes in two groups
817 were 14291 (0<dN/dS<1) and 1213 (dN/Ds>1), respectively.

818

819 **Fig. 5 Virulence genes were enriched in OC state.**

820 A. Chromatin state definitions, open chromatin (OC), strong transcription region (ST),
821 H3K9me3 dominant repression region (H3K9DR), H3K27me3 dominant repression

822 region (H3K27DR), quiescent state (Quies). B-C, genome coverage and composition
823 (emission probability) of histone marks and chromatin accessibility were presented. D,
824 Enrichments probability of different gene categories in each chromatin states measured
825 by chromHMM. E, Secretome genes were divided into CAZyme, CRN, SCR, NLP, RxLR
826 and other genes, and Sankey plot showed chromatin state distribution of those gene
827 groups. F, Percentage of gene in OC states compared with background group. Grey bars
828 were calculated as (gene number of corresponding gene group)/ (total gene number of *P.*
829 *infestans*). Purple color bars were calculated as (number of gene in corresponding gene
830 groups associated with OC state)/ (total number of genes associated in OC state). P-
831 value was calculated by Chi-squared test. G, Gene expression heatmap of OC state and
832 ST state associated secreted virulence genes in mycelium (MY), 2-day post incubation
833 (2 dpi) and 3-day post incubation (3 dpi) stages. Expression heatmap were normalized
834 by $\log_2$(FPKM+1) and clustered in row scale by Tbtools. H, Summary of percentage by
835 gene upregulation fold change in OC state and ST state associated secreted virulence
836 genes, the gene upregulation fold change was calculated using row FPKM value.

837

838 **S1 Fig. Sequences analysis of *P. infestans* H3 homologs.**

839 (A), Nucleotide sequences alignment of four *P. infestans* H3 homologs. **(**B), Amino acid
840 sequence alignment of four *P. infestans* H3 homologs.

S2 Fig. Phylogenetic and sequence analysis showed conserved Phytophthora H3 homologs.

(A), Phylogenetic analysis of Phytophthora H3 homologs. H3 homologs from human (HsH3.1/accession number: NP_003520.1, HsH3.2/ NP_066403.2, HsH3.3/NP_002098.1, HsCenP-A/NP_001035891.1), *Arabidopsis thaliana* (AtH3.1/NP_563838.1, AtH3.3/ NP_001329167.1, AtCenH3/NP_009564.1) and budding yeast(ScH3/NP_009564.1) were included in the study., H2A was set as an outgroup. (B), Alignment of H3 variants from *P. infestans* (PITG_05675 and PITG_03551) and *P. sojae* H3 (Ps_284752, Ps_322070 and Ps_476994) with HsH3.1, HsH3.2, AtH3.1, ScH3 and NcH3.

S3 Fig. PTM variants in Phytophthora H3.

(A), amino acid substitutions of two H3 forms were compared and different PTMs were marked. The numbers indicated amino acid position, amino acids at each site were listed and different colors indicated PTMs. (B), Individual mass spectrums of five PTM variants were shown.

S4 Fig. Summary of H3 lysine acetylation and methylation among seven organisms.

858 Highly conserved lysine were listed, red color indicated this PTM was detected or
859 reported, blue color indicated this PTM was not detected or reported. We used grey
860 color to mark the residue at 53 in human, for this site mutated to R.

861 **S5 Fig. H3K4me3, H3K9m3, H3K27me3 and H3K36me3 were detected in *P.***
862 ***infestans.***

863 (A), MS spectra of H3K4me3, H3K9m3, H3K27me3 and H3K36me3 in *P. infestans*. (B),
864 H3, H3K4me3, H3K9m3, H3K27me3 and H3K36me3 were detected by WB. *P. infestans*,
865 *P. sojae* and *M. oryzae* total protein were detected by five different antibodies, and
866 prokaryotic expressed H3 protein of *P. sojae* is the negative control that cannot be
867 modified.

868 **S6 Fig. The good quality and correlation between biological replicates of different**
869 **histone modifications and ATAC-seq in this study.**

870 (A). The overall analysis of ChIP-seq data and ATAC-seq data. (B). Highly repeatability
871 of two replicates. The genome was divided into 2kb bins and RPKM values of each bin
872 were used to calculate Pearson correlation coefficients. (C). Highly overlapped peak of
873 two replicates.

874 **S7 Fig. TE region have higher H3K9me3 and H3K27me3.**

875 **(**A). Methylation level of gene and TE were compared. Methylation level was calculated
876 as log2(IPRPKM/inputRPKM). P values are calculated with the two-sample Kolmogorov-

877 Smirnov test. (B). H3K9me3 and H3K27me3 are preferentially associated with LTR and
878 non-LTR type transposon in *P. infestans*. Intersected percentage of peaks length and TE
879 length were calculated.

880 **S8 Fig. PCA and heatmap clustering revealed overall distinct features between**
881 **ATAC-seq and ChIP-seq reads.**

882 PCA analysis (A) and heatmap clustering (B) of bw file generated by deepTools. each
883 dot represents one replicates. The Pearson correlation computation was used in (B).

884 **S9 Fig. Unique role of chromatin accessibility in chromatin state defining**
885 **compared with those four PTMs by peak analysis.**

886 ATAC peaks were divided into ATAC peak-alone, ATAC and H3K4me3 peak cobound,
887 and etc. The number of peaks were 10666, 3334, 1311, 2496, 1496, 331, 486 and 663,
888 respectively. Overlapped peaks defined in S6C Fig. were used here.

889 **S10 Fig. Genes under positive selection have higher H3K27me3 and H3K9me3 in**
890 ***P. infestans.***

891 (A), Conserved genes have lower dN/dS value, and *P. infestans* specific gene is under
892 highest positive selection. P values are calculated with the two-sample Kolmogorov-
893 Smirnov test. (B). GSR has higher dN/dS ratio. Gradient color represents dN/dS ratio.
894 (C), Genes under positive selection have higher H3K9me3 and H3K27me3. RPKM value
895 from -1 kb to 1 kb region of each gene were collected and the methylation level was

calculated as log2(IP_{RPKM}/$input_{RPKM}$). P values are calculated with the two-sample Kolmogorov-Smirnov test.

S11 Fig. Comparison of the GO enrichment result of methylated genes.

S12 Fig. Genes encoding secretome protein and RxLR effectors harbor higher H3K9me3 and H3K27me3, otherwise, ATAC-seq, H3K4me3 and H3K36me3 is lowly on these type of genes.

(A). comparison of ATAC-seq and four histone methylation signal in core, secretome and RxLR genes. P values are calculated with the two-sample Kolmogorov-Smirnov test. (B), Representative snapshot of silenced pectinase and RxLR gene cluster. The snapshot was collected from IGV software, and specific loci were marked by blue frame.

S13 Fig. GO enrichment result of genes in OC, ST, H3K9DR and H3K27DR chromatin states.

Fig. 1

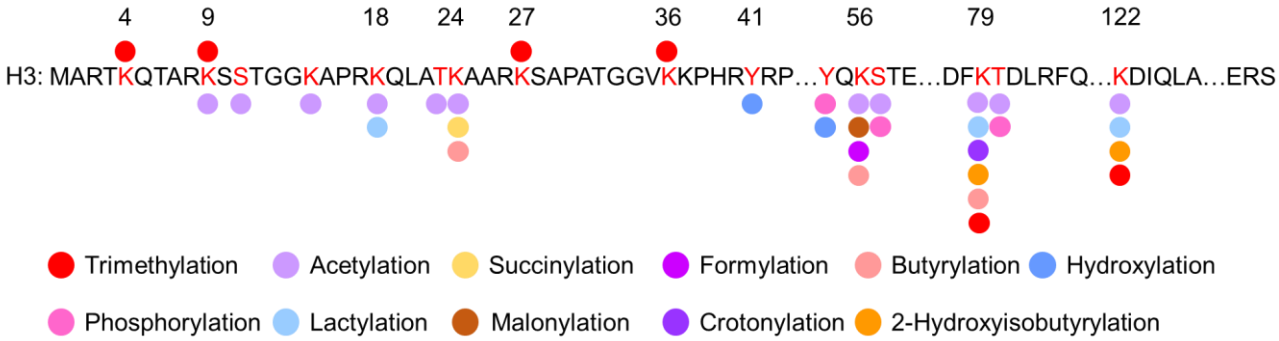

Fig. 2

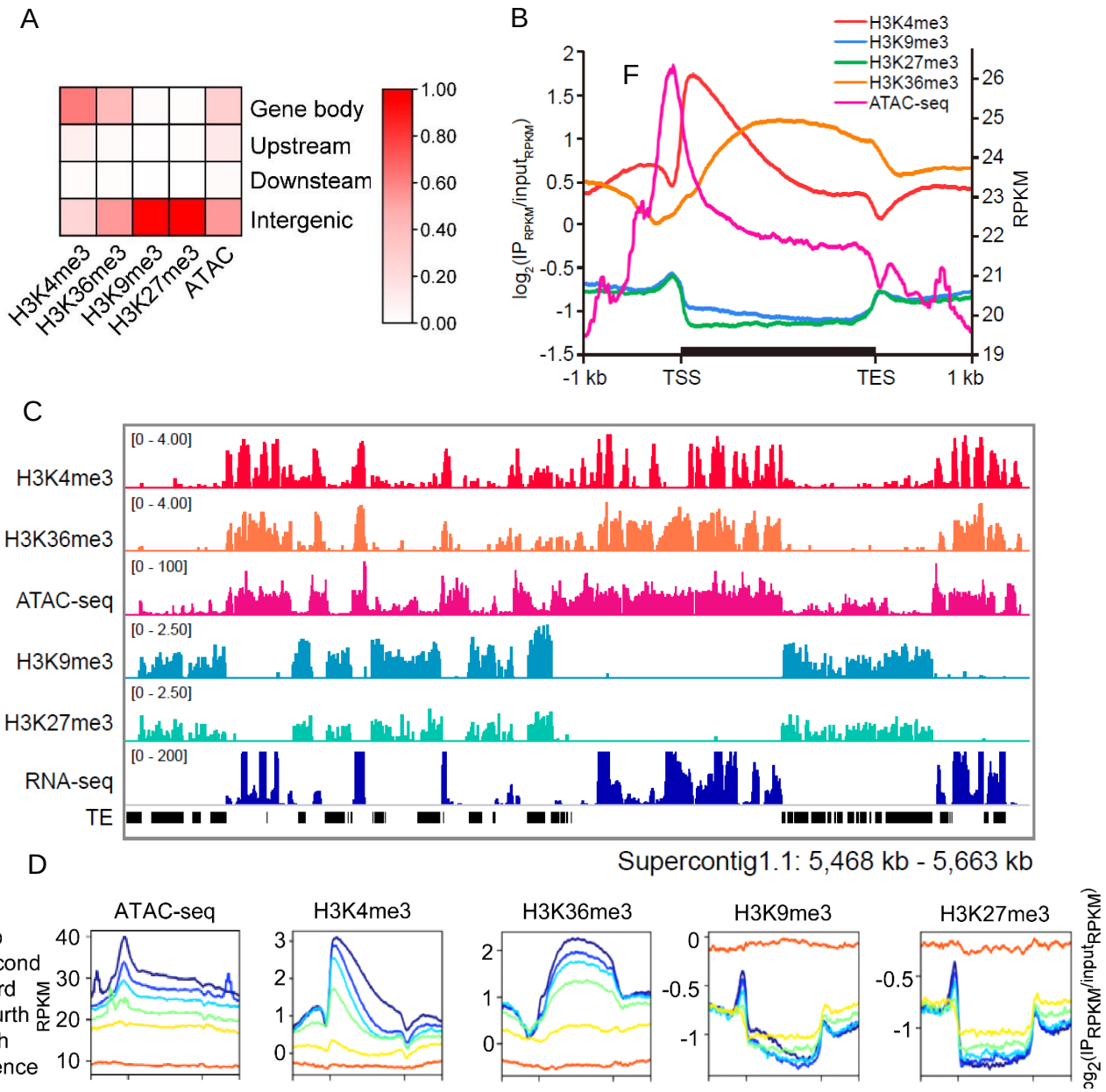

Fig. 3

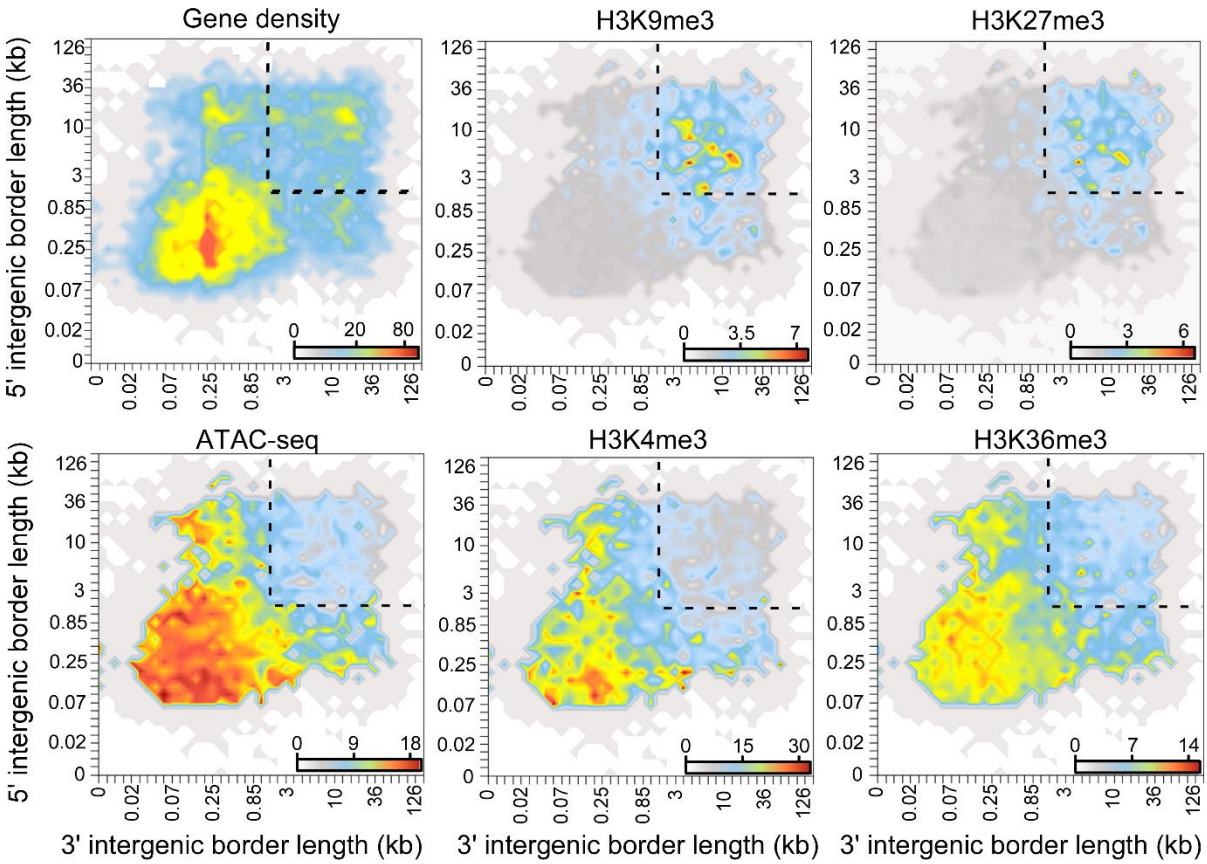

Fig. 4

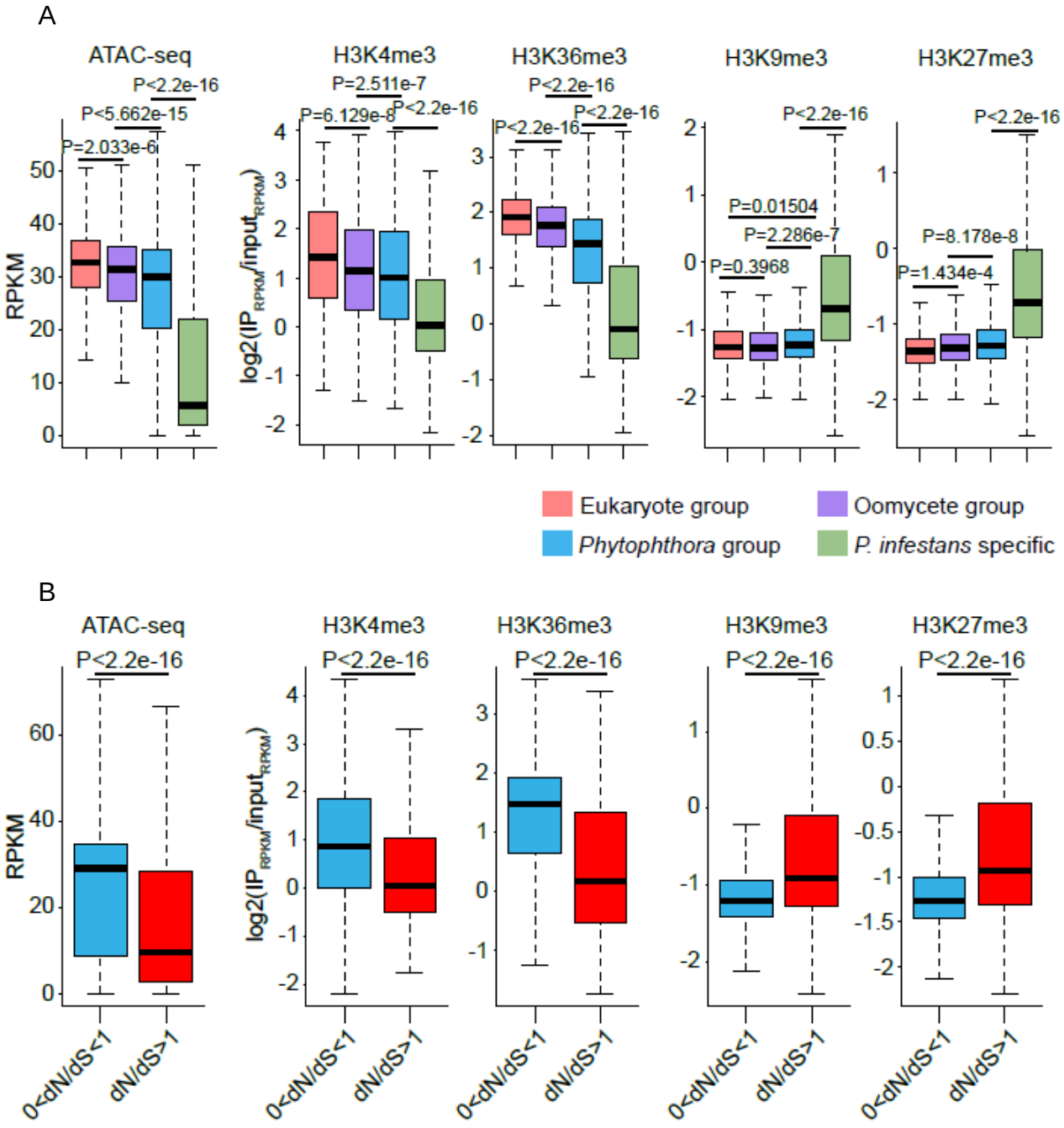

Fig. 5